Biochemistry

Article

Cite This: *Biochemistry* 2019, 58, 2608−2616

pubs.acs.org/biochemistry

A Noncanonical Chromophore Reveals Structural Rearrangements of the Light-Oxygen-Voltage Domain upon Photoactivation

Mindaugas E. Kalvaitis,[†] Luke A. Johnson,[†] Robert J. Mart,[†] Pierre Rizkallah,[‡] and Rudolf K. Allemann*[,†]

[†]School of Chemistry, Cardiff University, Park Place, Cardiff CF10 3AT, United Kingdom

[‡]School of Medicine, University Hospital Wales, Main Building, Heath Park, Cardiff CF14 4XN, United Kingdom

Supporting Information

ABSTRACT: Light-oxygen-voltage (LOV) domains are increasingly used to engineer photoresponsive biological systems. While the photochemical cycle is well documented, the allosteric mechanism by which formation of a cysteinyl-flavin adduct leads to activation is unclear. Via replacement of flavin mononucleotide (FMN) with 5-deazaflavin mononucleotide (5dFMN) in the Aureochrome1a (Au1a) transcription factor from *Ochromonas danica*, a thermally stable cysteinyl-5dFMN adduct was generated. High-resolution crystal structures (<2 Å) under different illumination conditions with either FMN or 5dFMN chromophores reveal three conformations of the highly conserved glutamine 293. An allosteric hydrogen bond network linking the chromophore via Gln293 to the auxiliary A′α helix is observed. With FMN, a "flip" of the Gln293 side chain occurs between dark and lit states. 5dFMN cannot hydrogen bond through the C5 position and proved to be unable to support Au1a domain dimerization. Under blue light, the Gln293 side chain instead "swings" away in a conformation distal to the chromophore and not previously observed in existing LOV domain structures. Together, the multiple side chain conformations of Gln293 and functional analysis of 5dFMN provide new insight into the structural requirements for LOV domain activation.

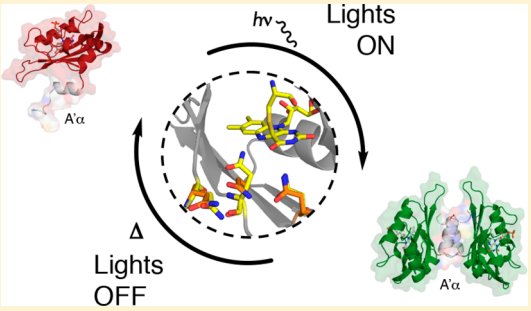

Light-oxygen-voltage (LOV) photoreceptors are members of the Per-ARNT-Sim (PAS) superfamily of proteins that act as blue-light-sensing modules, mediating a wide range of processes, including phototropism, circadian rhythms, and stress responses.[1−7] The modular arrangement of sensory LOV domain proteins and effectors found in nature[4,5,8−10] has inspired many synthetic designs.[11−16] Such engineered proteins exhibit varying levels of photoresponsiveness, which can be partly attributed to the incomplete understanding of the mechanisms of allosteric control employed by natural LOV domains over effector modules.[12,16−19] To fully exploit the photochemical potential of LOV domains for engineered systems, a comprehensive picture of the structural determinants of allostery is needed.

The structure of the LOV domain core is highly conserved, comprising a flavin chromophore binding site composed of a five-stranded, antiparallel β-sheet with ancillary helices.[7,20] Blue-light absorption results in the formation of reversible covalent adducts between the flavin isoalloxazine ring (C4a) and the sulfhydryl side chain of a conserved cysteine residue (Figure 1A). Flanking A′α (N-terminal) and Jα (C-terminal) helices act to relay photochemically induced changes in the LOV domain to associated effector modules.[21,22] Although the core LOV domain is structurally conserved, several different mechanisms of signal transduction are known. Mechanisms include Jα helix unfolding to release effector domains in *Avena sativa* phototropin 1 LOV2 (*As*LOV2),[23,24] Jα rotation and effector domain rearrangement in *Bacillus subtilis* YtvA (*Bs*YtvA),[25−27] and dimerization in *Neurospora crassa* vivid (*Nc*VVD).[6,28,29] The molecular basis of how such diverse results are obtained from the shared phenomenon of blue-light-driven formation of a covalent adduct between FMN and the cysteine side chain remains unclear.[7,20,28,30] One hypothesis suggests that protonation of N5 of the flavin cofactor, changing N5 from a hydrogen bond acceptor to a donor, causes a "flip" of the side chain of a conserved glutamine, with this change in polarity postulated to be communicated through a hydrogen bond donor/acceptor network.[31−33] The resolution of current crystal structures of lit-state proteins has been too low (>2.7 Å) to assert the rotamer identity with certainty.[29,34] Molecular dynamics (MD) simulations offer some support for the N5 protonation/glutamine flip hypothesis,[33] and site-directed mutagenesis of the glutamine residue confirmed its vital importance for the function of distantly related LOV domains,[28,32] suggesting a common underlying mechanism.

While the importance of the conserved glutamine is established, alternative hypotheses of how it governs light

Received: March 23, 2019
Revised: May 7, 2019
Published: May 13, 2019

DOI: 10.1021/acs.biochem.9b00255
Biochemistry 2019, 58, 2608−2616

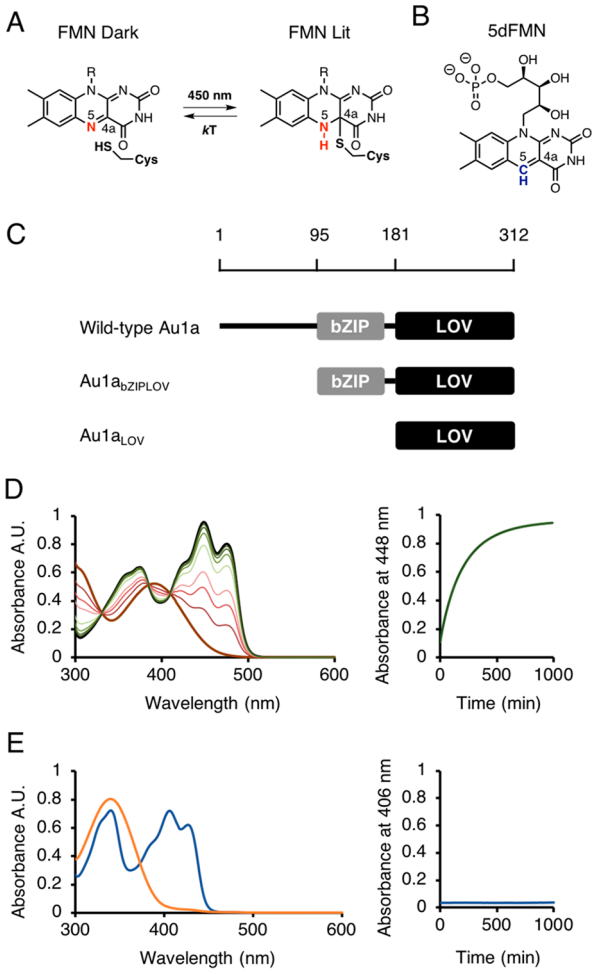

Figure 1. (A) Formation of a cysteinyl-FMN covalent adduct occurs upon absorption of blue light by flavin mononucleotide (FMN). Spontaneous thermal reversion re-forms the dark-adapted state. (B) Structure of 5-deazaflavin mononucleotide (5dFMN) with a carbon atom (blue) at position 5. (C) Domain topology of *O. danica* Aureochrome1a. Au1a$_{bZIPLOV}$ comprises bZIP and LOV domains, and Au1a$_{LOV}$ comprises only the LOV domain. UV−vis spectra of thermal reversion from the lit to dark state of (D) FMN-containing (red−green) and (E) 5dFMN-containing (orange−blue) *Od*Au1a$_{LOV}$. Spectra were recorded every hour for the first 3 h and then every 2 h. Reversion kinetics were monitored at 448 nm for FMN-containing *Od*Au1a$_{LOV}$ and 406 nm for 5dFMN-containing *Od*Au1a$_{LOV}$. Lit-state FMN *Od*Au1a$_{LOV}$ reverts to its dark state with a half-life of 112 min. No reversion to the dark state is observed for lit-state 5dFMN-containing *Od*Au1a$_{LOV}$.

switching have been proposed. MD simulations of phototropin LOV domains generated a different conformation for the conserved glutamine side chain, altering the hydrogen bonding network to flanking helices.[35−37] Other recent reports propose that further glutamine side chain orientations are involved in LOV domain activation through hydrogen bonds with O4 of the flavin ring.[37−40] Given the importance of the potential hydrogen bonding associated with N5 of the flavin and the challenges associated with studying the lit state of thermally reverting LOV domains, we used 5-deazaflavin mononucleotide [5dFMN (Figure 1B)], an analogue that had previously been suggested to form a stable photochemical cysteinyl-flavin adduct in *Bs*YtvA[41] and successfully employed to alter the redox potentials of other flavoproteins.[42−44] At present, there are no experimental data to indicate whether the lit states of 5dFMN-containing LOV photoreceptors function like FMN-containing examples. We therefore decided to examine the effect of 5dFMN incorporation on the photochemistry and function of Aureochrome1a (Au1a) of *Ochromonas danica*.

Aureochromes comprise a family of LOV domain-containing transcription factors found in photosynthetic stramenophiles that regulate the cell cycle and photomorphogenesis.[3,45,46] Au1a consists of an N-terminal unstructured region, followed by a basic leucine zipper (bZIP) domain and a C-terminal LOV domain. This domain topology is inverted compared to those of most other photoreceptors and means that the A′α helix, instead of the C-terminal Jα helix, connects effector and LOV domains. Spectroscopic and biochemical measurements of the isolated LOV domain from *Phaeodactylum tricornutum* and *Vaucheria frigida* Au1a suggest that stepwise unfolding of A′α and Jα helices upon illumination results in LOV domain dimerization.[22,47] Single-crystal X-ray structures of light-grown LOV domain crystals at 2.7 Å suggested the availability of the core β-sheet for use as a dimerization interface.[34] In dark-state structures, this dimerization site is obscured by the A′α helix. Full-length Au1a has resisted crystallization, but small-angle X-ray scattering (SAXS) of constructs whose unstructured region has been truncated shows significant volume changes that suggest intramolecular bZIP−LOV interactions.[34,46] Steric caging of the bZIP domain may therefore complement LOV domain-driven dimerization, which is proposed to be the driving force behind Aureochrome DNA binding.[48] Here, we present functional analysis and the first high-resolution crystal structures of a LOV domain with 5dFMN, identifying three conformations for Gln293 of Au1a and the allosteric network linking the chromophore to the A′α helix. This glutamine is widely conserved among LOV domains, and as there are several examples in which truncations of the A′α helix directly influence effectors connected through the Jα helix, these results may have wider implications beyond the Au1a family.

MATERIALS AND METHODS

Protein Expression and Purification. Standard molecular biology techniques were employed to generate *Od*Au1a$_{LOV}$ and *Od*Au1a$_{bZIPLOV}$ constructs from the wild-type *O. danica* Au1a gene (UniProt, C5NSW6_OCHDN) using oligonucleotides detailed in Table S1. *Od*Au1a-derived proteins were obtained by heterologous expression in BL21 (DE3) *Escherichia coli* in either minimal and autoinduction medium supplemented with glucose [1% (w/v)] and kanamycin (50−100 μg/mL). Cultures were grown at 37 °C until an OD_{600} of 0.8 was reached, induced with isopentenyl thiogalactose (0.5 mM, IPTG, Melford), and grown at 25 °C for a further 16 h. *Od*Au1a proteins were purified by Ni^{2+}-NTA (5 mL, GE Healthcare) affinity chromatography followed by Resource Q anion exchange (GE Healthcare) chromatography using purification buffer: 4-(2-hydroxyethyl)-1-piperazineethanesulfonic acid (HEPES, 20 mM, pH 7.8), sodium chloride [20 mM (*Od*Au1a$_{LOV}$) or 150 mM (*Od*Au1a$_{bZIPLOV}$)], triscarboxyethyl phosphine (TCEP, 0.3 mM), and gradients of imidazole (from 20 to 500 mM) and sodium chloride (from 0 to 1 M). Chromophore exchange was performed by applying the clarified cell lysate to Ni^{2+}-NTA resin (5 mL, GE Healthcare) and washing with 5 column volumes of purification buffer. Proteins were partially unfolded by passing this buffer supplemented with guanidine hydrochloride (6 M) over the resin. To complete FMN elution, a guanidinium thiocyanate

DOI: 10.1021/acs.biochem.9b00255
Biochemistry 2019, 58, 2608−2616

solution (3 M) was applied until no flavin was observed in the eluent by ultraviolet−visible (UV−vis) spectroscopy. Proteins were refolded by sequentially applying lower concentrations of guanidine hydrochloride (one column volumes of concentrations of 6, 5, 4, 3, 2, and 0 M). The resin was then washed with 5 column volumes of purification buffer, followed by incubation with 1 column volume of purification buffer containing 5dFMN (0.1−0.5 mM) for 30 min. Protein samples were eluted and then further purified as previously described.

Solution Characterization. For circular dichroism (CD) experiments, purified protein samples were dialyzed overnight at 4 °C against potassium phosphate buffer (10 mM, pH 7.0). Spectra were collected with an Applied Photophysics Chirascan spectrophotometer. For analytical gel filtration experiments, protein samples were exchanged into gel filtration buffer [HEPES (20 mM, pH 7.4), sodium chloride (100 mM), magnesium chloride (10 mM), and TCEP (0.3 mM)] in centrifugal filter columns. All protein samples were handled in dim red light. For photoactivation, protein samples were illuminated with 450 nm light-emitting diodes (LEDs) until a steady state was reached as determined by UV−vis spectroscopy. For gel filtration experiments, analytical gel filtration columns were either wrapped in aluminum foil for dark experiments or illuminated with 450 nm LEDs for lit-state experiments. For nuclear magnetic resonance (NMR) studies, purified and uniformly ^{15}N-labeled protein samples (400−600 μM) were exchanged into NMR buffer [2-(*N*-morpholino)-ethanesulfonic acid (MES, 20 mM, pH 6.0), ethylenediaminotetraacetate (EDTA, 1 mM), TCEP (1 mM), and sodium azide (0.05%)] and supplemented with 10% deuterium oxide. For dark-state experiments, protein samples were transferred into amber-colored NMR tubes. For lit-state experiments, protein samples were transferred into clear NMR tubes and illuminated with 450 nm LEDs. NMR spectra were recorded on a DPX-600 MHz Bruker NMR spectrometer equipped with a cryoprobe and preamplifiers.

DNA Binding. Light-dependent DNA binding was characterized by electrophoretic mobility gel shift assays (EMSAs) using TAMRA-labeled double-stranded DNA containing an *Od*Au1a recognition site (5′-TGTAGCGTC-TGACGTGGTTCCCAC-3′). EMSA experiments were performed at 4 °C. Dark-state experiments were performed in a room illuminated by dim red light, while for lit-state experiments, protein samples were illuminated for 5 min prior to commencing the experiment and throughout the electrophoresis experiment with 450 nm LEDs. Gels were imaged using a Bio-Rad ChemiDoc MP system (Bio-Rad Laboratories) and software provided by the manufacturer.

Crystallography. Purified FMN- or 5dFMN-containing *Od*Au1a$_{LOV}$ was exchanged into crystallization buffer [2-(*N*-morpholino)ethanesulfonate sodium salt (MES, 50 mM, pH 6.0), sodium chloride (100 mM), magnesium chloride (20 mM), sodium acetate (20 mM), dithiothreitol (DTT, 5 mM), and EDTA (5 mM)] and concentrated to 10−15 mg/mL. Dark-state crystals were grown in plates wrapped with aluminum foil by the hanging drop method. Drops consisted of protein (2 μL, 10 mg/mL) mixed with a reservoir solution [2 μL, 10−20% (w/v) polyethylene glycol (PEG) with an average molecular weight of 2000 or 3000, ammonium chloride (0.1 M), and sodium acetate (0.1 M, pH 4.5−4.9) or disodium citrate, (0.1 M, pH 4.5−4.9)] suspended over further reservoir buffer (100 μL) in 96-well plates (Screw Top Hanging Drop Plate, Molecular Dimensions). Crystal growth was usually evident after 16 h with maximum growth observed after 7 days. For dark-state structures, crystals were cryoprotected with ethylene glycol, harvested, and flash-frozen in liquid nitrogen under dim red light. For illumination experiments, crystals were illuminated with 450 nm LEDs for 30 min, cryoprotected with ethylene glycol, harvested, and flash-frozen in liquid nitrogen. Light-grown crystals were obtained by mixing light-state FMN- or 5dFMN-containing *Od*Au1a$_{LOV}$ (1.7 μL of a 15 mg/mL solution) with a reservoir solution [2 μL, disodium malonate (1.5−3 M, pH 7.0) and TRIS acetate (0.1 M, pH 7.5−8.0)]. Drops were supplemented with hexaamine cobalt(III) (0.3 μL, 0.1 M). Crystals were grown under blue light and appeared after 1−7 days. Crystals were harvested without cryoprotection and flash-frozen in liquid nitrogen. Data sets were collected from a single crystal each at the Diamond Light Source synchrotron at beamlines I02, I03, and I24. Initial structures were obtained from Phaser[55] or MolRep[55,56] using the dark-state *Phaeodactylum tricornum* Au1a$_{LOV}$ domain (Protein Data Bank entry 5A8B) as a search model. Structures were determined by subjecting initial models to cycles of model building with COOT[57] and refinement using REFMAC5.[55] For final R_{work} and R_{free} values, see Tables S4 and S5.

RESULTS

***Od*Au1a with 5dFMN Incorporated Forms a Thermally Stable Cysteinyl-Flavin Adduct.** To investigate the mechanism of LOV domain activation and the effects of introducing 5dFMN (Figure 1B), two truncated versions of *O. danica* Au1a containing the isolated LOV domain (*Od*Au1a$_{LOV}$) and the LOV domain with the DNA binding bZIP domain (*Od*Au1a$_{bZIPLOV}$) were constructed. The FMN cofactor of the expressed proteins was replaced with 5dFMN by binding the protein to Ni-NTA resin and washing with guanidine thiocyanate followed by removal of the denaturant and incubation with 5dFMN. Refolding of *Od*Au1a$_{LOV}$ and *Od*Au1a$_{bZIPLOV}$ in the presence of 5dFMN produced the characteristic blue-shifted vibrational triplet of oxidized 5dFMN with absorbance maxima at 385, 406, and 423 nm (Figure 1E and Figure S1C−F).[41] Comparing the absorbance at 406 and 475 nm indicated that >99% of the cofactor had been exchanged. *Od*Au1a$_{LOV}$ containing FMN reverted from its lit state to its dark state, with a half-life of 112 min, but no reversion was observed for *Od*Au1a$_{LOV}$ containing 5dFMN even after 7 days (Figure S1C,D). Cycling between lit and dark states using 450 and 330 nm light was possible with no significant photobleaching for at least five cycles (Figure S1E,F). The stability of the 5dFMN adduct was further demonstrated in liquid chromatography−mass spectrometry experiments in which species corresponding to the stable covalent cysteinyl-5dFMN conjugate for *Od*Au1a$_{LOV}$ were observed but no cysteinyl-FMN conjugates were evident (Figures S2 and S3).

FMN to 5dFMN Exchange Prevents Light-Induced Dimerization of *Od*Au1a$_{LOV}$. ^{1}H−^{15}N heteronuclear single-quantum coherence NMR spectra of ^{15}N-labeled proteins confirmed that refolding with 5dFMN did not lead to any large-scale structural perturbation. Illumination of *Od*Au1a$_{LOV}$ bound to 5dFMN resulted in chemical shift perturbations similar to those observed for FMN (Figure S4). CD spectra also indicated that the secondary structure after refolding of 5dFMN-containing *Od*Au1a$_{LOV}$ was the same as that of native *Od*Au1a$_{LOV}$ (Figure S5). Both FMN- and 5dFMN-containing

DOI: 10.1021/acs.biochem.9b00255
Biochemistry 2019, 58, 2608−2616

*Od*Au1a$_{LOV}$ samples exhibited changes in their CD spectra when photoactivated. FMN-containing *Od*Au1a$_{LOV}$ displayed a 14.2 ± 0.8% decrease in mean residue ellipticity at its 220 nm minimum (Figure 2A and Figure S5C), whereas 5dFMN-containing *Od*Au1a$_{LOV}$ exhibited a smaller change of 8.5 ± 1.0% at 220 nm (Figure 2B and Figure S5D). While UV−vis spectroscopy and mass spectrometry suggested complete and stable adduct formation for 5dFMN-containing *Od*Au1a$_{LOV}$, the secondary structural changes inferred an intermediate state. Size-exclusion chromatography was used to establish whether 5dFMN retained the capacity to induce *Od*Au1a$_{LOV}$ dimerization in response to light that has been shown for other isolated Aureochrome1a LOV domains.[21,22,49,50] FMN-containing *Od*Au1a$_{LOV}$ (100 μM) showed clear light-dependent dimerization as determined by size-exclusion chromatography. Dark-state FMN-containing *Od*Au1a$_{LOV}$ eluted at 13.7 mL with an estimated mass of 20.4 kDa with a slight shoulder toward a larger volume, whereas the lit-state equivalent elution maxima shifted to 12.8 mL in agreement with dimerization (Figure 2C). However, 100 μM 5dFMN-containing *Od*Au1a$_{LOV}$ showed very little shift of the elution volume with peaks at 13.5 and 13.3 mL for the dark and lit states, respectively (Figure 2D). Such an intermediate elution volume most likely represented a monomer−dimer exchange on the time scale of the size-exclusion experiments.

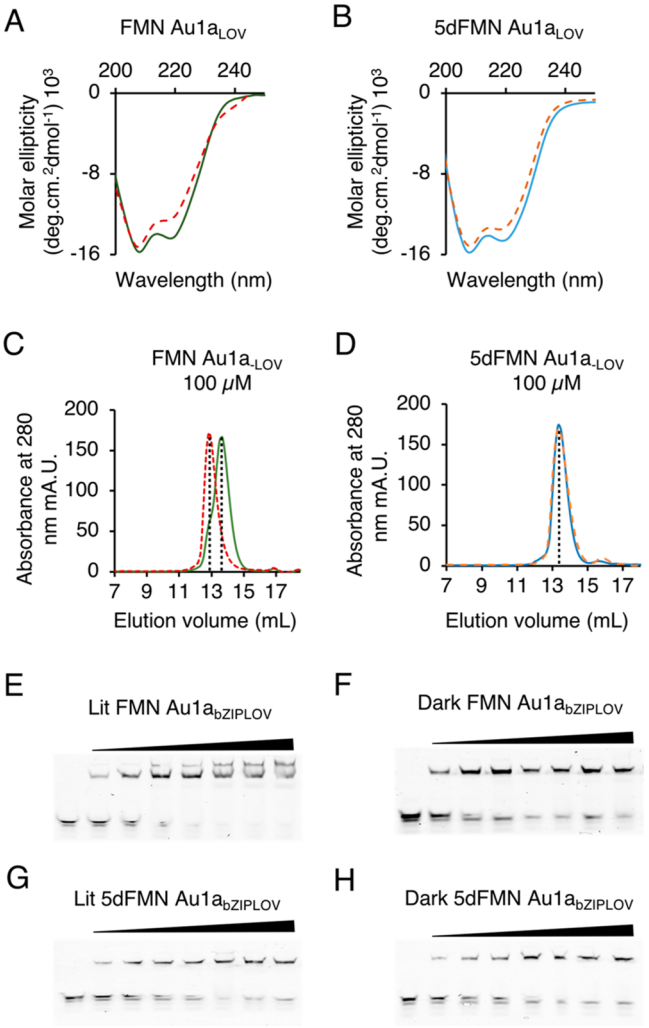

Figure 2. Circular dichroism spectra of (A) FMN-containing and (B) 5dFMN-containing *Od*Au1a$_{LOV}$ (20 μM) in potassium phosphate buffer (10 mM, pH 7.0) under dark and light (450 nm) conditions. Green and red traces correspond to dark and lit states of FMN, respectively, while blue and orange traces correspond to dark and lit states of 5dFMN, respectively. Size-exclusion chromatography of *Od*Au1a$_{LOV}$. (C) FMN-containing *Od*Au1a$_{LOV}$ under dark (green) and illuminated (red dashed) conditions. (D) 5dFMN-containing *Od*Au1a$_{LOV}$ under dark (blue) and illuminated (orange dashed) conditions. Electrophoresis mobility shift assays of *Od*Au1a$_{bZIPLOV}$ with a DNA target (40 nM) for (E) illuminated FMN-containing *Od*Au1a$_{bZIPLOV}$, (F) dark-state FMN-containing *Od*Au1a$_{bZIPLOV}$, (G) illuminated 5dFMN-containing *Od*Au1a$_{bZIPLOV}$, and (H) dark-state 5dFMN-containing *Od*Au1a$_{bZIPLOV}$. The first lane contains TAMRA-labeled DNA only, and subsequent lanes have increasing protein concentrations (from 0.4 to 12 μM from left to right, respectively).

To probe this observation further, we conducted concentration-dependent experiments. The position of the lit-state 5dFMN-containing *Od*Au1a$_{LOV}$ elution peak was strongly concentration-dependent (Figure S6), showing earlier elution at higher concentrations. In an identical concentration range, equivalent FMN-containing samples appeared to elute uniformly at volumes consistent with a dimer [200 to 10 μM (Figure S6)]. Although 5dFMN was unable to effect efficient dimerization in *Od*Au1a$_{LOV}$, the longer *Od*Au1a$_{bZIPLOV}$ construct consistently eluted from the size-exclusion column at volumes corresponding to a dimer with both cofactors in the dark and lit states (Figures S7−S9). Strong DNA binding was observed in both states regardless of the cofactor used for 50 μM protein samples. To further probe the light responsiveness of 5dFMN, lower concentrations were utilized in DNA binding assays.

Electrophoretic mobility shift assays were used to examine DNA binding by *Od*Au1a$_{bZIPLOV}$ containing FMN or 5dFMN in the dark and under illuminated conditions (Figure 2E−H). Lit-state FMN-containing *Od*Au1a$_{bZIPLOV}$ uniquely showed a slowly migrating "supershifted" band (Figure 2E),[46] while experiments with dark-state FMN (Figure 2F) and both dark and illuminated 5dFMN (Figure 2G,H) showed evidence of only a single slower-migrating shifted band. Having demonstrated by size-exclusion chromatography that FMN-containing *Od*Au1a$_{LOV}$ supports dimerization at 10 μM only when illuminated, the lower band may represent a 1:1 protein−DNA complex while the "supershifted" band most likely corresponds to the functional 2:1 complex of *Od*Au1a$_{bZIPLOV}$. The putative 2:1 complex was not observed when 5dFMN replaced FMN. Overall, the structural and functional experiments in solution suggest that 5dFMN incorporation creates a protein that can form a stable cysteinyl-5dFMN adduct that shows some structural features of a lit-state FMN-containing protein but with incomplete control over the longer-range interactions that direct DNA binding and dimer stability.

5dFMN Forms Cysteinyl-Flavin Adducts at the C4a Position but Induces No Rearrangement of the A′α Helix. To understand how 5dFMN can mimic FMN photochemistry but is incapable of complete *Od*Au1a activation, high-resolution single-crystal X-ray structures for FMN- and 5dFMN-containing *Od*Au1a$_{LOV}$ were determined for crystals grown in the dark, in the dark and then illuminated with blue light ("illuminated"), and under steady strong blue-light exposure ("light-grown"). The highest-resolution structure of dark-state FMN-containing *Od*Au1a$_{LOV}$ was obtained at 1.37 Å from a single crystal in space group $P2_12_12_1$ with four monomers per asymmetric unit as parallel dimers (Figure 3A).

DOI: 10.1021/acs.biochem.9b00255
Biochemistry 2019, 58, 2608−2616

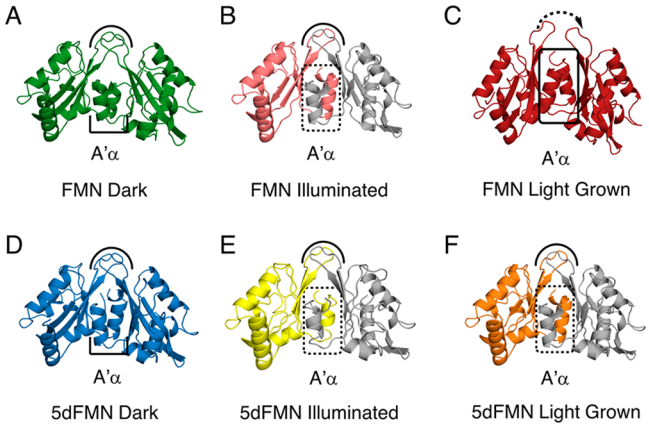

Figure 3. Dimer arrangements for X-ray crystal structures of FMN- and 5dFMN-containing *Od*Au1a$_{LOV}$ under dark (left), illuminated (middle), and light-grown (right) conditions. (A) The 1.37 Å structure of dark-state FMN-containing *Od*Au1a. The asymmetric unit contained four monomers as parallel dimers (green) with A′α positioned across the β-sheet surface (half black box). Loops of each monomer lie close to each other (black curved line). (B) The 1.50 Å structure of illuminated crystals of dark-grown FMN-containing *Od*Au1a. The asymmetric unit contained a single monomer (pink), forming a parallel dimer similar to that in the dark state when considering a symmetry equivalent (gray). (C) The 1.66 Å structure of light-grown FMN-containing *Od*Au1a featuring a unique dimer arrangement with A′α being repositioned across a β-sheet surface (black box) and loop region rearrangement (dashed arrow). (D) The 1.97 Å structure of dark-state 5dFMN-containing *Od*Au1a with a dimer similar to dark-state FMN. (E) The 1.43 Å structure of illuminated 5dFMN-containing *Od*Au1a with a symmetry partner equivalent to a dimer colored gray. (F) The 2.00 Å structure of light-grown 5dFMN-containing *Od*Au1A showing a similar loop (black curved line) and A′α helix arrangement (black box) as for dark-state and illuminated proteins with a symmetry equivalent colored gray.

Crystals in space group $P3_121$ were also observed, but these diffracted poorly. A 1.97 Å structure of dark-state 5dFMN-containing *Od*Au1a$_{LOV}$ was obtained from crystals grown under identical conditions in space group $P3_121$ indicating a parallel dimer per asymmetric unit (Figure 3D). The identity of the cofactor had little effect on the overall LOV domain structure or the chromophore binding pocket (Figure 4A,D), confirming an identical mode of chromophore binding and no rearrangement of the surrounding environment. When dark-grown crystals were illuminated, the space group changed to $P6_422$ with a single monomer per asymmetric unit (Figure 3B,E). However, once symmetry partners were considered, symmetrical dimers almost identical to the dark-adapted state could be identified with symmetry equivalents. Inspection of the cofactor binding site of the illuminated crystals showed electron density for approximately 30% occupancy of a covalent bond between Cys230 and the cofactor for both FMN and 5dFMN structures (Figure 4B,E). This occupancy that is significantly lower than indicated by UV−vis spectroscopy and MS (Figure 1D,E, and S10) is likely to be the result of a photochemical scission of the covalent adduct during data collection as reported for other LOV domain proteins.[29] Although the usual approach under such circumstances is to record multiple data sets from a single crystal, this usually yields much poorer resolution and was therefore not attempted. We hypothesized that higher-resolution data sets could provide unique insights into structural change. To ensure minimal bias in the cycles of structural refinement, we modeled covalent adduct structure at 30% occupancy (cysteinyl-flavin photoadduct) and the dark state at 70% occupancy, yielding two flavin and cysteine orientations. Electron density for a partial occupancy of a cysteinyl-flavin adduct at the C4a position of the isoalloxazine ring for 5dFMN-containing *Od*Au1a$_{LOV}$ was clearly observed, confirming that 5dFMN forms a photochemical adduct structurally equivalent to the native chromophore.

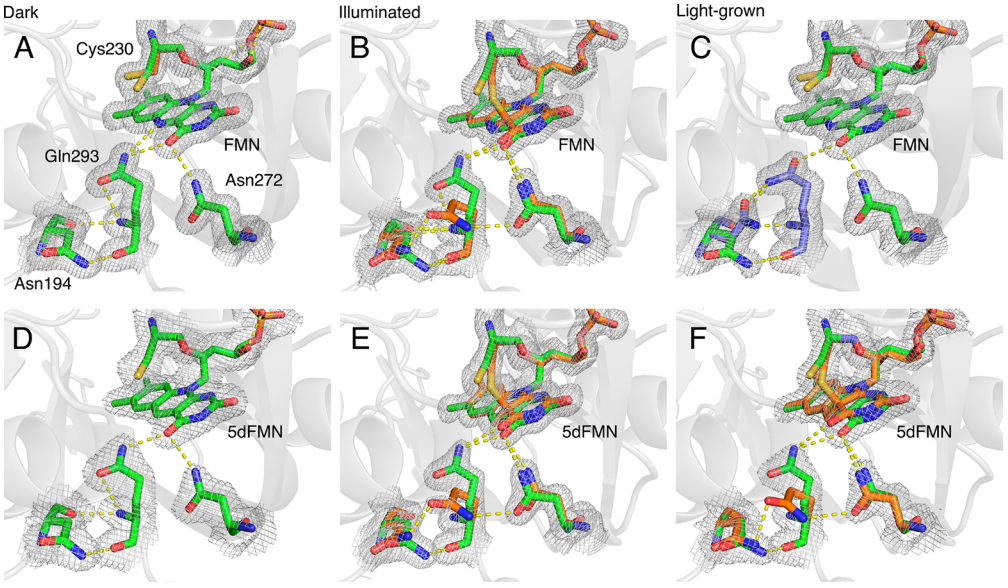

Figure 4. Electron density maps (gray mesh) for FMN or 5dFMN, Cys230, and residues forming hydrogen bonding networks among O4 of FMN, Asn272, Gln293, and Asn194 are displayed at the σ = 1 level. Partial occupancies are colored by characteristic conformations observed for dark-state (green), illuminated (orange), or light-grown (purple) structures. Yellow dashed lines indicate predicted hydrogen bonding. (A) Dark-state FMN (1.36 Å). (B) Illuminated FMN (1.50 Å). (C) Light-grown FMN (1.67 Å). (D) Dark-state 5dFMN (1.97 Å). (E) Illuminated 5dFMN (1.43 Å). (F) Light-grown 5dFMN (2.00 Å).

DOI: 10.1021/acs.biochem.9b00255
Biochemistry 2019, 58, 2608−2616

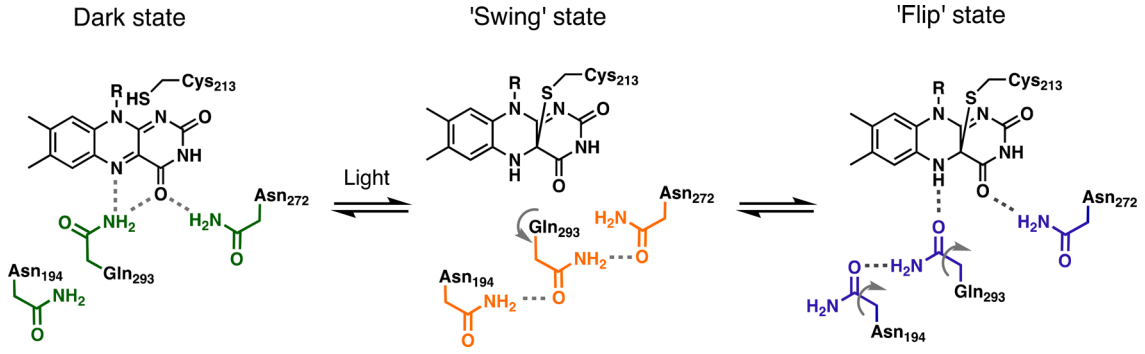

Figure 5. In the dark-state conformation (green), conserved Gln293 hydrogen bonds to O4 and N5 of FMN. Illumination with blue light results in the Gln293 "swing" state (orange) where its side chain rotates away from the FMN chromophore. Progression to the Gln293 "flip" state (purple) may occur from the "swing" state or from the dark state but cannot proceed when the protein is trapped in the crystal lattice. Rotation of the side chain of Asn194 upon formation of the "flip" state is likely to lead to conformational changes in the A′α helix.

Light-grown crystals could not be obtained under the conditions used for the dark state, but alternative conditions produced monoclinic crystals in space group *C*121 for the FMN sample and hexagonal crystals in space group $P6_422$ for 5dFMN. For light-grown FMN-containing *Od*Au1a$_{LOV}$, no cysteinyl-FMN adduct was evident in the electron density map. Electron density corresponding to a cysteinyl-5dFMN adduct was observed but was less prominent than in maps from illuminated crystals. Notably, light-grown FMN-containing *Od*Au1a$_{LOV}$ contained four monomers per asymmetric unit as parallel dimers. Two of the monomers appeared to be identical to the dark-state structure, while the second pair showed a different A′α arrangement across the β-sheet surface. Compared with the dark-state structures, a change in the relative positions of strand Iβ (287−293) of the β-sheet and A′α (183−189) of 12° is observed. This rearrangement does not occur in illuminated structures, probably due to crystal lattice constraints. Light-grown 5dFMN-containing *Od*Au1a$_{LOV}$ maintained a single monomer per asymmetric unit, resembling the arrangement of illuminated structures. This supported solution data that although 5dFMN undergoes photochemistry similar to that of FMN, it is unable to fully activate *Od*Au1a$_{LOV}$. Taken together, this suggests that the A′α rearrangement, observed for only light-grown FMN-containing *Od*Au1a$_{LOV}$, could correlate with dimerization in solution (Figure 3A,C).

Adduct Formation Populates Different Conformations of Gln293. Dark-state structures gave single well-defined populations of Gln293, Asn272, and Asn194 for both FMN and 5dFMN, but close examination of electron density maps from illuminated and light-grown conditions yielded multiple conformations for these residues (Figure 4). In dark-state structures, Gln293 lies close to the chromophore and forms a probable hydrogen bond to the O4 position (Figure 4A,D). For illuminated structures, a 20% occupancy of a new conformation of Gln$_{293}$, with its side chain away from the FMN binding pocket, was evident (Figure S22). Additional conformations of Asn194 and Asn272 are also observed. Formation of a new hydrogen bond network among these three residues creates a route for the conformation of Gln293 to be communicated to the A′α helix through Asn194 (Figure 4B,E), which is located in the loop connecting A′α with the LOV domain core. Examination of the FMN binding pocket of the light-grown crystal structure revealed a third arrangement for Gln293 and Asn194. In the parallel dimer with a unique A′α arrangement, Asn194 moves in toward Gln293. This coincides with a probable change in the orientation of the Gln293 side chain and the polarity of the hydrogen bond network due to flavin protonation (Figure 4C). In contrast, 5dFMN-containing *Od*Au1a$_{LOV}$ did not form this "flip" conformation but closely resembled the structure of illuminated 5dFMN-containing *Od*Au1a$_{LOV}$ with identical Asn194 and Gln293 conformations (Figure 4F). This suggests that the structural changes that we observed were not an artifact of different crystallization conditions, as identical space groups were achieved for 5dFMN under both conditions. It appears that only growing crystals of FMN-containing protein under constant illumination allow the structural reorientation of the allosteric A′α helix to support dimer rearrangement (Figure 3).

DISCUSSION

Reconstitution of truncated versions of the light-dependent transcription factor *Od*Au1a$_{LOV}$ with 5dFMN led to proteins that undergo photoadduct formation to produce a thermally stable cysteinyl-5dFMN adduct. Despite clear evidence of adduct formation captured by UV spectroscopy and mass spectrometry and subsequent light-induced changes determined by CD and NMR spectroscopy, 5dFMN-containing *Od*Au1a$_{LOV}$ does not dimerize under the conditions where dimerization of FMN *Od*Au1a$_{LOV}$ occurs. High-resolution crystal structures show identical FMN and 5dFMN binding modes in dark-grown crystals, suggestive of identical chromophore binding characteristics. Crystal structures of illuminated and light-grown *Od*Au1a$_{LOV}$ containing 5dFMN provide conclusive evidence of cysteinyl photoadduct formation at the C4a position in apparent support of the radical-based mechanism proposed for the native chromophore.[41]

Crystal structures obtained under different illumination conditions define three distinct conformations for conserved Gln293 and its hydrogen bonding partners. For the FMN-containing light-grown crystal structure, inspection of calculated difference maps with both rotamers strongly implies a glutamine "flip" (Figure S22). Protonation of FMN and a corresponding "flip" of the glutamine side chain is a leading hypothesis for LOV activation[29,32,33] and has even been used to explain the activation of a LOV domain containing a neutral semiquinone flavin.[51] However, in our and other published light-grown structures,[29,34] the distance between Gln293 and N5 of FMN is longer than might be expected for a hydrogen bond (~3.3 Å). 5dFMN forms the equivalent covalent adduct, but in contrast to FMN, Gln293 does not appear to "flip" in

DOI: 10.1021/acs.biochem.9b00255
Biochemistry 2019, 58, 2608−2616

light-grown crystals (Figure 4C,F). Taken with 5dFMN's inability to induce light-dependent dimerization, this furthermore suggests that N5 protonation is a prerequisite for locking the lit-state conformation of *Od*Au1a$_{LOV}$. Comparison of illuminated and light-grown FMN-containing *Od*Au1a$_{LOV}$ structures (Figure 4B,C) suggests that a key aspect of the Gln293 "flip" is to engage an alternative conformation of the side chain of Asn194, located between the Aβ strand and A′α helix, in hydrogen bonding. This change in the Asn194 conformation may be the key to propagating the effects of adduct formation beyond the LOV domain, by rearranging the domain to favor dimerization and/or by releasing the A′α helix. Notably, this key Asn residue is also found in other Au1a homologues[34,49,50] and in *As*LOV2.[52]

To the best of our knowledge, our structures of illuminated crystals of 5dFMN-containing *Od*Au1a$_{LOV}$ provide the first experimental evidence for a further arrangement of Gln293 and Asn194. For both FMN and 5dFMN, Gln293 "swings" away from the chromophore when illuminated (Figure 5). The persistence of a "swing" conformation in 5dFMN light-grown crystals suggests that it is not a crystallographic artifact generated by illuminating LOV domains trapped in the crystal lattice or a product of a different space group due to changes in crystallographic conditions but that 5dFMN is unable to support progress to the "flip" state. CD measurements indicate that illumination of 5dFMN-containing OdAu1aLOV results in some secondary structural changes, although not to the extent seen with FMN. Likewise, size-exclusion chromatography revealed intermediate changes upon illumination for 5dFMN. These results infer the "swing" conformation of Gln293, formed in the absence of larger-scale secondary structural changes, provides a degree of activation. It therefore seems probable that the "swing" state represents an intermediate stage in activation rather than an unproductive conformation (Figure 5).

The key determinants of success for LOV domain-based optogenetic systems are the dynamic ranges of affinities and activities in the dark and lit states. Most previous work has relied on using molecular modeling to guide alterations to helix docking propensities to improve the dynamic range of optogenetic tools. Here we provide experimental insight into the molecular basis of LOV domain photoactivation. The nature of the "swing" state may be crucial for improving LOV domains by rational design; if the "swing" state is an on-path intermediate, then encouraging its formation is of key importance, placing a greater emphasis on the O4−Gln293−Asn194 axis for initial activation. This is in agreement with MD simulations and Fourier transform infrared spectroscopy experiments that identified hydrogen bond changes to O4 of the FMN ring being important for the regulation of LOV domain activation especially in the early stages after photoadduct formation.[35−37,39,40] Indeed, results that inferred a role for N5 protonation by generation of a neutral flavin semiquinone radical[33,51] and N5-protonated reduced flavins[53] also predict significant polarity changes at O4.[54] Alternatively, if the "swing" state is an off-path intermediate, its destabilization may lead to improved switches with higher dynamic ranges. Understanding these fundamental aspects of domain activation has a potentially enormous impact for the design of new tools based on LOV domains and may allow researchers to improve the performance of designed LOV domains with multiple optogenetic applications.

■ ASSOCIATED CONTENT

Supporting Information

The Supporting Information is available free of charge on the ACS Publications website at DOI: 10.1021/acs.biochem.9b00255.

Experimental procedures, including purification, characterization, and crystallization methods; UV−vis spectroscopy, mass spectrometry, NMR, CD, and SEC data of *Od*Au1a (Figures S1−S10, S22) and 5-deazaflavin mononucleotide chemoenzymatic synthesis (Figures S11−S21); and tables of DNA oligonucleotides, protein sequences, and structural refinement statistics (Tables S4 and S5) (PDF)

Accession Codes

Protein Data Bank entries 6I20, 6I21, 6I22, 6I23, 6I24, and 6I25.

■ AUTHOR INFORMATION

Corresponding Author

*E-mail: allemannrk@cardiff.ac.uk.

ORCID

Mindaugas E. Kalvaitis: 0000-0002-8175-7552
Luke A. Johnson: 0000-0002-6697-6589
Robert J. Mart: 0000-0003-2196-5840
Pierre Rizkallah: 0000-0002-9290-0369
Rudolf K. Allemann: 0000-0002-1323-8830

Funding

This work was supported by BBSRC Grants BB/M006158/1 and BB/P009980/1 and EPSRC Grant EP/L027240/1.

Notes

The authors declare no competing financial interest.

■ ACKNOWLEDGMENTS

The authors thank Dr. Harald Janovjak (IST Austria) for providing the DNA encoding full-length *O. danica* Aureochrome1a, Dr. Yi Jin for help with structure determination and helpful discussions, and Tom Williams for assistance with mass spectrometry. The authors thank the Diamond Light Source for beamtime (Proposal mx14843) and the staff of beamlines I02, I03, and I24 for assistance with data collection.

■ ABBREVIATIONS

*Od*Au1a, *O. danica* Aureochrome1a; LOV, light-oxygen-voltage; bZIP, basic leucine zipper; FMN, flavin mononucleotide; PAS, Per-ARNT-Sim; 5dFMN, 5-deazaflavin mononucleotide; CD, circular dichroism; SAXS, small-angle X-ray scattering; MD, molecular dynamics; NMR, nuclear magnetic resonance.

■ REFERENCES

(1) Crosson, S., Rajagopal, S., and Moffat, K. (2003) The LOV Domain Family: Photoresponsive Signaling Modules Coupled to Diverse Output Domains. *Biochemistry 42*, 2−10.

(2) Ito, S., Song, Y. H., and Imaizumi, T. (2012) LOV Domain-Containing F-Box Proteins: Light-Dependent Protein Degradation Modules in Arabidopsis. *Mol. Plant 5*, 573−582.

(3) Krauss, U., Minh, B. Q., Losi, A., Gärtner, W., Eggert, T., Von Haeseler, A., and Jaeger, K. E. (2009) Distribution and Phylogeny of Light-Oxygen-Voltage-Blue-Light-Signaling Proteins in the Three Kingdoms of Life. *J. Bacteriol. 191*, 7234−7242.

DOI: 10.1021/acs.biochem.9b00255
Biochemistry 2019, 58, 2608−2616

(4) Glantz, S. T., Carpenter, E. T., Melkonian, M., Gardner, K. H., Boyden, E. S., Wong, G. K., and Chow, B. Y. (2016) Functional and Topological Diversity of LOV Domain Photoreceptors. *Proc. Natl. Acad. Sci. U. S. A. 113*, E1442−E1451.
(5) Bonomi, H. R., Posadas, D. M., Paris, G., Carrica, M. D. C., Frederickson, M., Pietrasanta, L. I., Bogomolni, R. A., Zorreguieta, A., and Goldbaum, F. A. (2012) Light Regulates Attachment, Exopolysaccharide Production, and Nodulation in Rhizobium Leguminosarum through a LOV-Histidine Kinase Photoreceptor. *Proc. Natl. Acad. Sci. U. S. A. 109*, 12135−12140.
(6) Chen, C. H., DeMay, B. S., Gladfelter, A. S., Dunlap, J. C., and Loros, J. J. (2010) Physical Interaction between VIVID and White Collar Complex Regulates Photoadaptation in Neurospora. *Proc. Natl. Acad. Sci. U. S. A. 107*, 16715−16720.
(7) Möglich, A., Ayers, R. A., and Moffat, K. (2009) Structure and Signaling Mechanism of Per-ARNT-Sim Domains. *Structure 17*, 1282−1294.
(8) Cao, Z., Buttani, V., Losi, A., and Gärtner, W. (2008) A Blue Light Inducible Two-Component Signal Transduction System in the Plant Pathogen Pseudomonas Syringae Pv. Tomato. *Biophys. J. 94*, 897−905.
(9) Purcell, E. B., Siegal-Gaskins, D., Rawling, D. C., Fiebig, A., and Crosson, S. (2007) A Photosensory Two-Component System Regulates Bacterial Cell Attachment. *Proc. Natl. Acad. Sci. U. S. A. 104*, 18241−18246.
(10) Herrou, J., and Crosson, S. (2011) Function, Structure and Mechanism of Bacterial Photosensory LOV Proteins. *Nat. Rev. Microbiol. 9*, 713−723.
(11) Christie, J. M., Gawthorne, J., Young, G., Fraser, N. J., and Roe, A. J. (2012) LOV to BLUF: Flavoprotein Contributions to the Optogenetic Toolkit. *Mol. Plant 5*, 533−544.
(12) Strickland, D., Moffat, K., and Sosnick, T. R. (2008) Light-Activated DNA Binding in a Designed Allosteric Protein. *Proc. Natl. Acad. Sci. U. S. A. 105*, 10709−10714.
(13) Mart, R. J., Meah, D., and Allemann, R. K. (2016) Photocontrolled Exposure of Pro-Apoptotic Peptide Sequences in LOV Proteins Modulates Bcl-2 Family Interactions. *ChemBioChem 17*, 698−701.
(14) Niopek, D., Wehler, P., Roensch, J., Eils, R., and Di Ventura, B. (2016) Optogenetic Control of Nuclear Protein Export. *Nat. Commun. 7*, 10624.
(15) Renicke, C., Schuster, D., Usherenko, S., Essen, L. O., and Taxis, C. (2013) A LOV2 Domain-Based Optogenetic Tool to Control Protein Degradation and Cellular Function. *Chem. Biol. 20*, 619−626.
(16) Lee, J., Natarajan, M., Nashine, V. C., Socolich, M., Vo, T., Russ, W. P., Benkovic, S. J., and Ranganathan, R. (2008) Surface Sites for Engineering Allosteric Control in Proteins. *Science 322*, 438−442.
(17) Strickland, D., Yao, X., Gawlak, G., Rosen, M. K., Gardner, K. H., and Sosnick, T. R. (2010) Rationally Improving LOV Domain Based Photoswitches. *Nat. Methods 7*, 623−626.
(18) Gehrig, S., Macpherson, J. A., Driscoll, P. C., Symon, A., Martin, S. R., MacRae, J. I., Kleinjung, J., Fraternali, F., and Anastasiou, D. (2017) An Engineered Photoswitchable Mammalian Pyruvate Kinase. *FEBS J. 284*, 2955−2980.
(19) Kawano, F., Suzuki, H., Furuya, A., and Sato, M. (2015) Engineered Pairs of Distinct Photoswitches for Optogenetic Control of Cellular Proteins. *Nat. Commun. 6*, 6256.
(20) Crosson, S., and Moffat, K. (2001) Structure of a Flavin-Binding Plant Photoreceptor Domain: Insights into Light-Mediated Signal Transduction. *Proc. Natl. Acad. Sci. U. S. A. 98*, 2995−3000.
(21) Herman, E., Sachse, M., Kroth, P. G., and Kottke, T. (2013) Blue-Light-Induced Unfolding of the Jalpha Helix Allows for the Dimerization of Aureochrome-LOV from the Diatom Phaeodactylum Tricornutum. *Biochemistry 52*, 3094−3101.
(22) Herman, E., and Kottke, T. (2015) Allosterically Regulated Unfolding of the A'alpha Helix Exposes the Dimerization Site of the Blue-Light-Sensing Aureochrome-LOV Domain. *Biochemistry 54*, 1484−1492.
(23) Harper, S. M., Christie, J. M., and Gardner, K. H. (2004) Disruption of the LOV-Jalpha Helix Interaction Activates Phototropin Kinase Activity. *Biochemistry 43*, 16184−16192.
(24) Harper, S. M., Neil, L. C., and Gartner, K. H. (2003) Structural Basis of a Phototrophin Light Switch. *Science 301*, 1541−1544.
(25) Möglich, A., and Moffat, K. (2007) Structural Basis for Light-Dependent Signaling in the Dimeric LOV Domain of the Photosensor YtvA. *J. Mol. Biol. 373*, 112−126.
(26) Berntsson, O., Diensthuber, R. P., Panman, M. R., Björling, A., Hughes, A. J., Henry, L., Niebling, S., Newby, G., Liebi, M., Menzel, A., Henning, R., Kosheleva, I., Möglich, A., and Westenhoff, S. (2017) Time-Resolved X-Ray Solution Scattering Reveals the Structural Photoactivation of a Light-Oxygen-Voltage Photoreceptor. *Structure 25*, 933−938.
(27) Engelhard, C., DIensthuber, R. P., Möglich, A., and Bittl, R. (2017) Blue-Light Reception through Quaternary Transitions. *Sci. Rep. 7*, 1385.
(28) Zoltowski, B. D., Schwerdtfeger, C., Widom, J., Loros, J. J., Bilwes, A. M., Dunlap, J. C., and Crane, B. R. (2007) Conformational Switching in the Fungal Light Sensor Vivid. *Science 316*, 1054−1057.
(29) Vaidya, A. T., Chen, C. H., Dunlap, J. C., Loros, J. J., and Crane, B. R. (2011) Structure of a Light-Activated LOV Protein Dimer That Regulates Transcription. *Sci. Signaling 4*, ra50.
(30) Diensthuber, R. P., Bommer, M., Gleichmann, T., and Möglich, A. (2013) Full-Length Structure of a Sensor Histidine Kinase Pinpoints Coaxial Coiled Coils as Signal Transducers and Modulators. *Structure 21*, 1127−1136.
(31) Jones, M. A., Feeney, K. A., Kelly, S. M., and Christie, J. M. (2007) Mutational Analysis of Phototropin 1 Provides Insights into the Mechanism Underlying LOV2 Signal Transmission. *J. Biol. Chem. 282*, 6405−6414.
(32) Nash, A. I., Ko, W. H., Harper, S. M., and Gardner, K. H. (2008) A Conserved Glutamine Plays a Central Role in LOV Domain Signal Transmission and Its Duration. *Biochemistry 47*, 13842−13849.
(33) Ganguly, A., Thiel, W., and Crane, B. R. (2017) Glutamine Amide Flip Elicits Long Distance Allosteric Responses in the LOV Protein Vivid. *J. Am. Chem. Soc. 139*, 2972−2980.
(34) Heintz, U., and Schlichting, I. (2016) Blue Light-Induced LOV Domain Dimerization Enhances the Affinity of Aureochrome 1a for Its Target DNA Sequence. *eLife 5*, No. e11860.
(35) Freddolino, P. L., Dittrich, M., and Schulten, K. (2006) Dynamic Switching Mechanisms in LOV1 and LOV2 Domains of Plant Phototropins. *Biophys. J. 91*, 3630−3639.
(36) Peter, E., Dick, B., and Baeurle, S. A. (2010) Mechanism of Signal Transduction of the LOV2-Jα Photosensor from Avena Sativa. *Nat. Commun. 1*, 122.
(37) Freddolino, P. L., Gardner, K. H., and Schulten, K. (2013) Signaling Mechanisms of LOV Domains: New Insights from Molecular Dynamics Studies. *Photochem. Photobiol. Sci. 12*, 1158−1170.
(38) Pudasaini, A., Shim, J. S., Song, Y. H., Shi, H., Kiba, T., Somers, D. E., Imaizumi, T., and Zoltowski, B. D. (2017) Kinetics of the LOV Domain of ZEITLUPE Determine Its Circadian Function in Arabidopsis. *eLife 6*, e21646.
(39) Gil, A. A., Laptenok, S. P., French, J. B., Iuliano, J. N., Lukacs, A., Hall, C. R., Sazanovich, I. V., Greetham, G. M., Bacher, A., Illarionov, B., Fischer, M., Tonge, P. J., and Meech, S. R. (2017) Femtosecond to Millisecond Dynamics of Light Induced Allostery in the Avena Sativa LOV Domain. *J. Phys. Chem. B 121*, 1010−1019.
(40) Zayner, J. P., Antoniou, C., and Sosnick, T. R. (2012) The Amino-Terminal Helix Modulates Light-Activated Conformational Changes in As LOV2. *J. Mol. Biol. 419*, 61−74.
(41) Mansurova, M., Scheercousse, P., Simon, J., Kluth, M., and Gärtner, W. (2011) Chromophore Exchange in the Blue Light-Sensitive Photoreceptor YtvA from Bacillus Subtilis. *ChemBioChem 12*, 641−646.
(42) Fisher, J., Spencer, R., and Walsh, C. (1976) Enzyme-Catalyzed Redox Reactions with the Flavin Analogues 5-Deazariboflavin, 5-

DOI: 10.1021/acs.biochem.9b00255
Biochemistry 2019, 58, 2608−2616

Deazariboflavin 5′-Phosphate, and 5-Deazariboflavin 5′-Diphosphate, 5′ →5′-Adenosine Ester. *Biochemistry 15*, 1054−1064.
(43) Hemmerich, P., Massey, V., and Fenner, H. (1977) Flavin and 5-Deazaflavin: A Chemical Evaluation of "modified" Flavoproteins with Respect to the Mechanisms of Redox Biocatalysis. *FEBS Lett. 84*, 5−21.
(44) Hedison, T. M., Leferink, N. G. H., Hay, S., and Scrutton, N. S. (2016) Correlating Calmodulin Landscapes with Chemical Catalysis in Neuronal Nitric Oxide Synthase Using Time-Resolved FRET and a 5-Deazaflavin Thermodynamic Trap. *ACS Catal. 6*, 5170−5180.
(45) Takahashi, F., Yamagata, D., Ishikawa, M., Fukamatsu, Y., Ogura, Y., Kasahara, M., Kiyosue, T., Kikuyama, M., Wada, M., and Kataoka, H. (2007) AUREOCHROME, a Photoreceptor Required for Photomorphogenesis in Stramenopiles. *Proc. Natl. Acad. Sci. U. S. A. 104*, 19625−19630.
(46) Banerjee, A., Herman, E., Serif, M., Maestre-Reyna, M., Hepp, S., Pokorny, R., Kroth, P. G., Essen, L. O., and Kottke, T. (2016) Allosteric Communication between DNA-Binding and Light-Responsive Domains of Diatom Class 1 Aureochromes. *Nucleic Acids Res. 44*, 5957−5970.
(47) Herman, E., Sachse, M., Kroth, P. G., and Kottke, T. (2013) Blue-Light-Induced Unfolding of the J-Alpha Helix Allows for the Dimerization of Aureochrome-LOV from the Diatom Phaeodactylum Tricornutum. *Biochemistry 52*, 3094−3101.
(48) Akiyama, Y., Nakasone, Y., Nakatani, Y., Hisatomi, O., and Terazima, M. (2016) Time-Resolved Detection of Light-Induced Dimerization of Monomeric Aureochrome-1 and Change in Affinity for DNA. *J. Phys. Chem. B 120*, 7360−7370.
(49) Mitra, D., Yang, X., and Moffat, K. (2012) Crystal Structures of Aureochrome1 LOV Suggest New Design Strategies for Optogenetics. *Structure 20*, 698−706.
(50) Banerjee, A., Herman, E., Kottke, T., and Essen, L. O. (2016) Structure of a Native-like Aureochrome 1a LOV Domain Dimer from Phaeodactylum Tricornutum. *Structure 24*, 171−178.
(51) Yee, E. F., Diensthuber, R. P., Vaidya, A. T., Borbat, P. P., Engelhard, C., Freed, J. H., Bittl, R., Möglich, A., and Crane, B. R. (2015) Signal Transduction in Light-Oxygen-Voltage Receptors Lacking the Adduct-Forming Cysteine Residue. *Nat. Commun. 6*, 10079.
(52) Halavaty, A. S., and Moffat, K. (2007) N- and C-Terminal Flanking Regions Modulate Light-Induced Signal Transduction in the LOV2 Domain of the Blue Light Sensor Phototropin 1 from Avena Sativa. *Biochemistry 46*, 14001−14009.
(53) Purcell, E. B., McDonald, C. A., Palfey, B. A., and Crosson, S. (2010) An Analysis of the Solution Structure and Signaling Mechanism of LovK, a Sensor Histidine Kinase Integrating Light and Redox Signals. *Biochemistry 49*, 6761−6770.
(54) Lans, I., Frago, S., and Medina, M. (2012) Understanding the FMN Cofactor Chemistry within the Anabaena Flavodoxin Environment. *Biochim. Biophys. Acta, Bioenerg. 1817*, 2118−2127.
(55) Winn, M. D., Ballard, C. C., Cowtan, K. D., Dodson, E. J., Emsley, P., Evans, P. R., Keegan, R. M., Krissinel, E. B., Leslie, A. G. W., McCoy, A., McNicholas, S. J., Murshudov, G. N., Pannu, N. S., Potterton, E. A., Powell, H. R., Read, R. J., Vagin, A., and Wilson, K. S. (2011) Overview of the CCP4 Suite and Current Developments. *Acta Crystallogr., Sect. D: Biol. Crystallogr. 67*, 235−242.
(56) Vagin, A. A., Steiner, R. A., Lebedev, A. A., Potterton, L., McNicholas, S., Long, F., and Murshudov, G. N. (2004) REFMAC 5 Dictionary: Organization of Prior Chemical Knowledge and Guidelines for Its Use. *Acta Crystallogr., Sect. D: Biol. Crystallogr. 60*, 2184−2195.
(57) Emsley, P., Lohkamp, B., Scott, W. G., and Cowtan, K. (2010) Features and development of Coot. *Acta. Crystallogr. D Biol. Crystallogr. 66*, 486−501.

DOI: 10.1021/acs.biochem.9b00255
Biochemistry 2019, 58, 2608−2616